Improved Uniformity of Superconducting Properties in GdBCO Superconductor Bulk with a Buffer Layer

Y. Zhang[a], Y.F. Zhang[a,*], S.Y. Shen[a], W.L. Wang[a], G.J. Ruan[a], Y. Li[a], J.Y. Zhang[a], P.H. Zhang[a], Z.W. Lou[a], L. Peng[a] and D.F. Zhou[b]

[a] *College of Mathematics and Physics, Shanghai University of Electric Power, 1851 Hucheng Ring Road, New Pudong District, Shanghai 201306, People's Republic of China*
[b] *Shanghai Key Laboratory of High Temperature Superconductors, Shanghai University, 99 Shangda Road, Baoshan District, Shanghai 200444, People's Republic of China*

Received: 02.03.2024 & Accepted: 29.05.2024

Doi: 10.12693/APhysPolA.146.195 *e-mail: 2009000018@shiep.edu.cn

Uneven distribution of local superconducting properties can significantly impact the overall performance of $REBa_2Cu_3O_{7-\delta}$ (REBCO or RE123) superconductor bulks. Through the modified top-seeded melt-texture growth method, we successfully prepared single-domain $GdBa_2Cu_3O_{7-\delta}$ (GdBCO) superconductor bulks with (bulk A) and without (bulk B) a buffer layer, and investigated the relationship between superconducting properties and microstructure of the bulks in detail. Measurement results show that the maximum trapped flux density value of bulk A is 0.48 T, and that of bulk B is 0.5 T. The distribution of transition temperature (T_C) and critical current density (J_C) becomes more uniform along the c- and a/b-directions in bulk A. In bulk B, i.e., without a buffer layer, the J_C varies greatly at different locations due to microstructural inhomogeneity. The buffer layer acting as a large seed can increase the growth rate, resulting in a decrease in the size and an increase in the concentration of Gd_2BaCuO_5 (Gd211) particles in the microstructure according to pushing/trapping and coarsening theory. The corresponding J_C performance shows a certain improvement in all fields, which suggests that the buffer layer has a positive effect on the spatial uniformity of superconducting properties in superconductor bulks.

topics: GdBCO superconductor bulk, top-seeded melt-texture growth (TSMG) method, critical current density, buffer layer

1. Introduction

High-temperature superconductors, such as $REBa_2Cu_3O_{7-\delta}$ (REBCO or RE123, where RE represents rare earth elements, like Y, Gd, Sm, Nd, etc.), exhibit superior magnetic field trapping capabilities and higher critical current density compared to low-temperature superconductors. This makes them more suitable for practical applications in production and daily life. High-temperature superconductors have already had a significant impact on practical applications such as maglev trains, flywheel energy storage systems, and superconducting bearings [1–5]. Currently, there are two main methods for preparing REBCO superconductors: top-seeded melt-texture growth (TSMG) and top-seeded infiltration and growth (TSIG). TSMG has been widely studied due to its convenience and effectiveness [6, 7]. However, traditional TSMG can cause sample shrinkage due to diffusion and loss of the liquid phase, leading to decreased superconductivity or sample preparation failure [8, 9]. In contrast, TSIG can reduce sample shrinkage by introducing a liquid phase source, which ensures a sufficient amount of liquid phase to the precursor pellet [10]. To address this issue, RE123 pellets were introduced as a liquid phase source in the TSMG process, resulting in a modified TSMG.

In the 1990s, buffer layer technology emerged as a versatile method for various purposes in high-performance coated conductor production: relieving lattice mismatch stress, overcoming strong diffusion of cations, minimizing film–substrate reactions, and promoting texture growth of highly c-axis-oriented REBCO phase [11–14]. Over time, buffer-assisted technology has become recognized as an effective means to enhance high-temperature superconductor performance [15–18]. The buffer layer acts as a protective barrier against contamination from crystal seeds, enhances the thermal stability of seeds,

and serves as a large seed for growing large REBCO superconductors. Consequently, buffer layer technology [19–22] has seen rapid development and gained widespread attention. Li et al. [23] demonstrated that combining buffer layer technology with the TSMG method could suppress Mg and Sm diffusion in seed material, leading to a higher critical transition temperature (T_C) in the specimens located near film seeds compared to those in the bulk without the buffer layer. Namburi et al. [24] investigated the effect of different buffer layer compositions and aspect ratios on superconductivity and found that buffer particles can improve the superconducting properties and thermal stability of crystal seeds. Furthermore, it was suggested that buffer layers could serve as large seeds to promote nucleation and growth of the Y123 phase at reduced costs while producing larger diameter samples.

The equation $B_{\text{trap}} = A\mu_0 J_C R$ (where A is a constant and μ_0 is the permeability of vacuum) reveals that the trapped flux density B_{trap} in high-temperature superconductor bulks is directly proportional to the critical current density J_C and the radius R of single-domain superconductor bulks. However, factors such as micro- and macro-cracks, subgrain boundaries, dislocations, and Gd211 particle distribution [25, 26] usually adversely affect the J_C properties. Nano-sized non-superconducting defects or dopants in the superconducting RE123 phase substrate can also impact J_C by acting as effective flux pinning centers. Recent studies have shown that porosity has a detrimental effect on J_C, with no significant correlation found between RE_2BaCuO_5 (RE211) particle distribution and localized J_C in GdBCO bulks. Baumann et al. [27] used three-dimensional (3D) X-ray computer tomography (XCT) and a superconducting quantum interference device (SQUID) to investigate the effect of porosity on J_C in superconductor bulks. Their results indicate that reducing porosity on the micron scale enhances J_C. To improve the quality and superconducting properties of REBCO superconductors, it is crucial to explore the relationship between microstructure and superconducting properties. This paper presents the successful preparation of two types of GdBCO superconductor bulks with and without a buffer layer using the modified TSMG method. By measuring critical transition temperature T_C, critical current density J_C, and scanning electron microstructure (SEM) maps at different locations within the bulks, we analyzed the relationship between superconducting properties and microstructure. Our results show that the introduction of a buffer layer leads to a more concentrated distribution of the critical transition temperature T_C and a more consistent J_C profile at different locations. The distribution of Gd211 particles in the microstructure suggests that this improvement in uniformity is primarily due to the addition of a buffer layer, which facilitates the uniformity of superconducting properties in bulks.

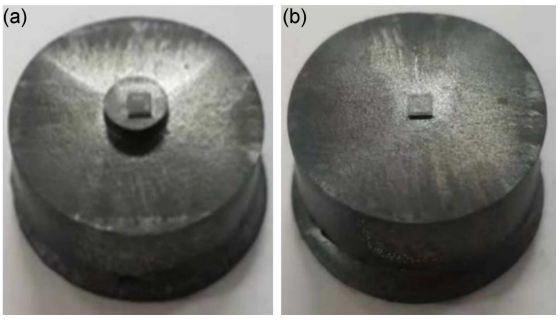

Fig. 1. Top view of GdBCO superconductor bulks with (a) and without (b) a buffer layer.

2. Experimental details

Commercially pure powders of $GdBa_2Cu_3O_{7-\delta}$ (Gd123) (99.9%) and Gd_2BaCuO_5 (Gd211) (99.9%) were mixed in a molar ratio of Gd123 : Gd211 = 4 : 1. After mixing thoroughly with a mortar, the powders were pressed into a cylinder pellet with a diameter of 6 mm and a thickness of 3 mm, which served as the buffer layer. In order to improve the mechanical properties of the bulks and refine the Gd211 particles, 10 wt% of Ag_2O and 0.5 wt% of Pt were added afterward, and then pressed into a pellet with a diameter of 25 mm and a thickness of 12 mm, which served as the precursor. Commercially pure powder of $YBa_2Cu_3O_{7-\delta}$ (Y123) was pressed into a pellet with the diameter of 25 mm and the thickness of 3 mm, which was placed under the precursor as the liquid phase source. The NdBCO seed crystals based on MgO substrate with dimensions of $2 \times 2 \times 0.5$ mm^3 were placed at the center of the buffer layer, which was then placed on the upper surface of the precursor. In addition, the 5 g of Y_2O_3 was pressed into a pellet with a diameter of 25 mm and placed under the liquid phase source to prevent the reaction with the Al_2O_3 substrate. Meanwhile, we fabricated another GdBCO precursor without the buffer layer under the same conditions. NdBCO seed crystals were placed directly on the upper surface of the precursor to guide the growth of the superconductor bulk. For ease of differentiation, we labeled superconductor bulks with the buffer layer as bulk A and those without the buffer layer as bulk B. Two arrangements were placed in a box furnace for the modified TSMG process. Temperature was first rapidly raised from room temperature to 1080°C and held for 1 h. Then, it was rapidly lowered to 1009°C and slowly cooled down to 979°C at a 0.3°C/h rate. Finally, the temperature was cooled to room temperature within 10 h. At the end of the sintering, the samples were annealed in the high-purity oxygen flow. The samples were heated to 450°C in 5 h and held for 40 h, then cooled to

TABLE I

Specimens, dimensions (width — a, length — b, height — c), and masses of bulk A and bulk B.

Specimens	bulk A		bulk B	
	Dimensions $a/b/c$ of the specimens [mm]	Masses of the specimens [mg]	Dimensions $a/b/c$ of the specimens [mm]	Masses of the specimens [mg]
c1	1.64/1.70/0.96	19.6	1.70/2.06/1.00	25.0
c2	1.74/1.74/0.98	21.1	1.66/1.84/1.00	20.8
c3	1.58/1.74/0.96	19.3	1.74/2.00/0.96	23.4
c4	1.68/1.84/0.92	20.0	1.52/2.10/0.90	20.5
b1	1.58/1.84/0.92	19.8	1.74/1.98/0.90	23.2
a1	1.98/2.08/0.96	23.8	1.68/1.78/0.96	20.3
s1	1.96/2.08/0.84	22.7	1.70/1.80/0.94	19.5
t1	1.80/2.06/0.90	21.3	1.50/1.82/0.96	16.4
b3	1.78/1.78/1.00	22.8	1.64/1.78/0.96	16.5
a3	1.82/2.02/1.00	21.5	1.70/1.80/1.00	20.6
s3	1.66/1.78/0.92	19.7	1.80/1.82/0.96	18.5
t3	1.88/1.94/0.92	20.2	1.80/1.84/0.94	20.4

400°C in 40 h, to 300°C in 100 h, and finally cooled naturally to room temperature. The growth bulks are shown in Fig. 1.

For the measurement of trapped flux density, the samples were cooled down to the liquid nitrogen temperature under a magnetic field of 1.5 T. The applied magnetic field was removed after 30 min, and then the trapped flux density distribution was measured using a Hall probe sensor, with the probe kept 0.5 mm from the sample surface. In order to investigate the relationship between microstructure and superconducting properties, we cut the samples into small specimens of $2 \times 2 \times 1$ mm^3 along the c-direction and a/b-direction, respectively. The specific cutting positions are shown in Fig. 2, where four specimens, labeled c1, c2, c3, and c4, were cut along the c-direction directly below the seeds, and four specimens, labeled b1, a1, s1, and t1, were cut from the seed to the edge of the bulks along the a/b-direction starting from the c1 position. Similarly, four specimens, labeled b3, a3, s3, and t3, were cut from the seed to the edge of the sample along the a/b-direction starting from position c3. The dimensions (width — a, length — b, height — c) and masses of the specimens in bulk A and bulk B are shown in Table I. The DC magnetization measurements of the specimens were carried out using the physical property measurement system (PPMS), and the critical current densities were calculated from the extended Bean critical state model [28]. According to the formula

$$J_C = \frac{20\Delta M}{aV\left(1-\frac{a}{3b}\right)}, \tag{1}$$

where a and b are the width and length of the specimens with $a \leq b$, V is the volume of the specimens, and ΔM is the difference between positive and negative magnetic moments. The microstructure was observed through the scanning electron microscope (SEM).

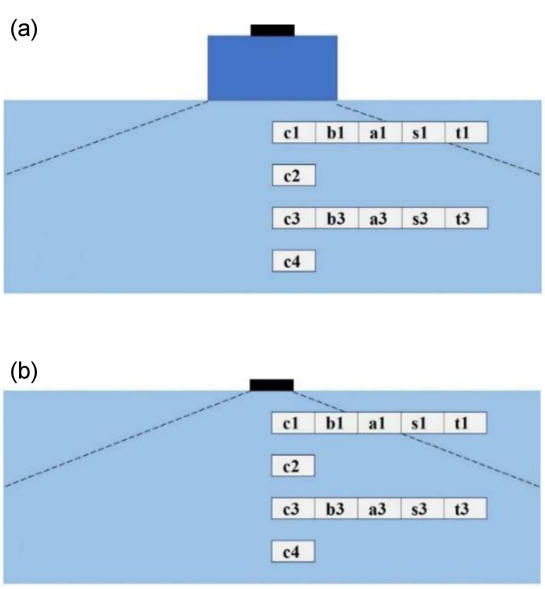

Fig. 2. Schematic diagram of the positions of all specimens cut from the GdBCO superconductor bulks with (a) and without (b) a buffer layer.

3. Results and discussion

Figure 1 shows the growth results of two single-domain GdBCO superconductor bulks fabricated by the modified TSMG process with (a) and

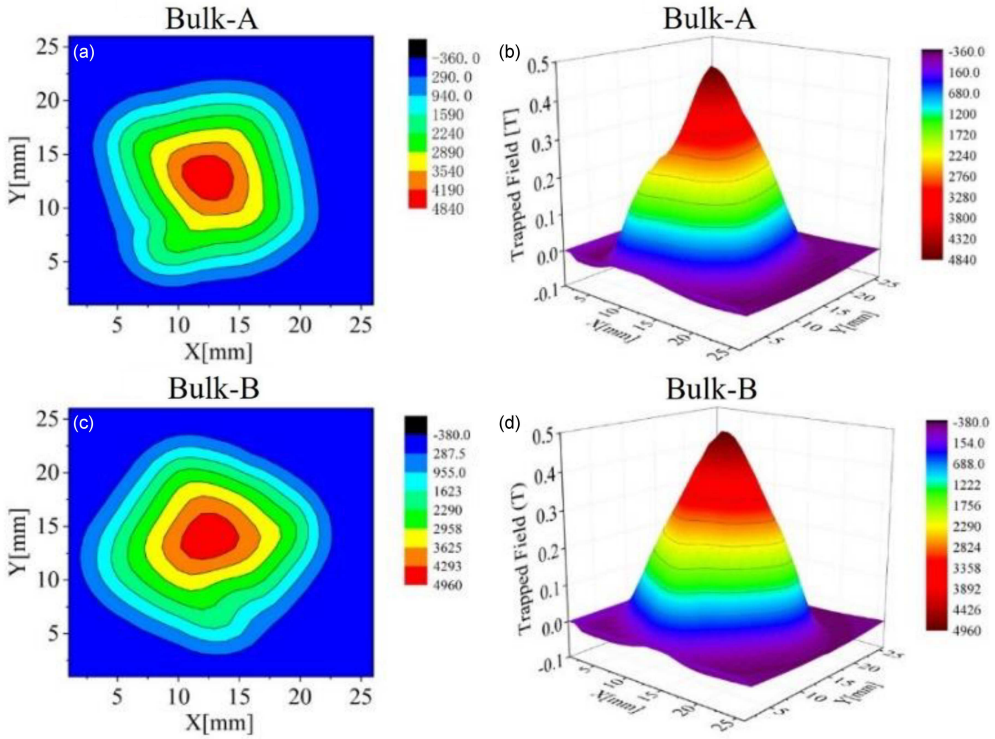

Fig. 3. The top surface trapped field (3D map and 2D map) of GdBCO superconductor bulks with (bulk A) and without (bulk B) the buffer layer. (a) 2D map of bulk A; (b) 3D map of bulk A; (c) 2D map of bulk B; (d) 3D map of bulk B.

without (b) a buffer layer. NdBCO seed crystals of two GdBCO bulks are not melted, and the four-fold growth facet lines can be clearly observed, which indicates the successful preparation of the GdBCO superconductor bulks. With the addition of the buffer layer, the growth of the superconductor bulk induces the buffer layer first from the seed and then from the main pellet. Such a buffer-assisted seeding architecture can reduce the depth of the grain boundary formed by the top surface and the a/c-growth sector boundaries (a/c-GSBs), thus reducing the a-growth sector (a-GS) volume and increasing the c-growth sector (c-GS) volume [29–31]. Diko et al. [32] found that in superconductor bulks prepared using the TSMG method, Y211 and solidified liquid phases tend to accumulate near the growth sector boundaries (GSBs), leading to impaired superconductivity near the GSBs. The increase in c-GS volume in the bulk implies the decrease in a/c-GSBs and non-superconducting phases, so it is favorable for the superconducting properties.

Figure 3 shows the trapped flux density of bulk A with a buffer layer and bulk B without a buffer layer. It is clear that the quadrilateral circle of bulk A is more symmetrical than the triangular circle of bulk B in a two-dimensional (2D) view. As shown in Fig. 3a and c, trapped magnetic fields with good symmetry usually indicate a uniform distribution of superconducting properties, therefore we predict that bulk A with a buffer layer has more uniform superconducting properties. The trapped field profiles of bulk A and bulk B exhibit conical shapes as well as a single peak, meaning that the samples constitute a single-domain bulk. The maximum trapped flux density values measured by the Hall probe sensor are 0.48 T in bulk A with a buffer layer and 0.50 T in bulk B without a buffer layer. The small difference in their trapped field suggests that the addition of the buffer layer does not damage the superconducting properties of GdBCO bulk.

Figure 4a and b shows the temperature dependence of magnetization of specimens c1, c2, c3, and c4 below the seeds in, respectively, bulk A with a buffer layer and bulk B without a buffer layer in a zero-field-cooling (ZFC) mode under 10 Oe applied fields with $H \parallel c$-axis. It can be seen that all specimens have the onset transition temperature T_C values higher than 94 K, indicating excellent superconducting properties for both bulks. The onset T_C increases with increasing distance along the c-direction in bulk A (Fig. 4a), where the c3 specimen has the largest onset T_C of 94.8 K. Compared with bulk B, the T_C distribution in bulk A is more concentrated, and all specimens maintain a narrower transition width. Bulk B (Fig. 4b) has a more dispersed distribution of onset T_C values, with the c1 specimen below the seed having the smallest onset T_C value, i.e., 95.1 K, and the c4 specimen at the bottom having the largest onset T_C value, i.e., 95.8 K. The critical temperature T_C

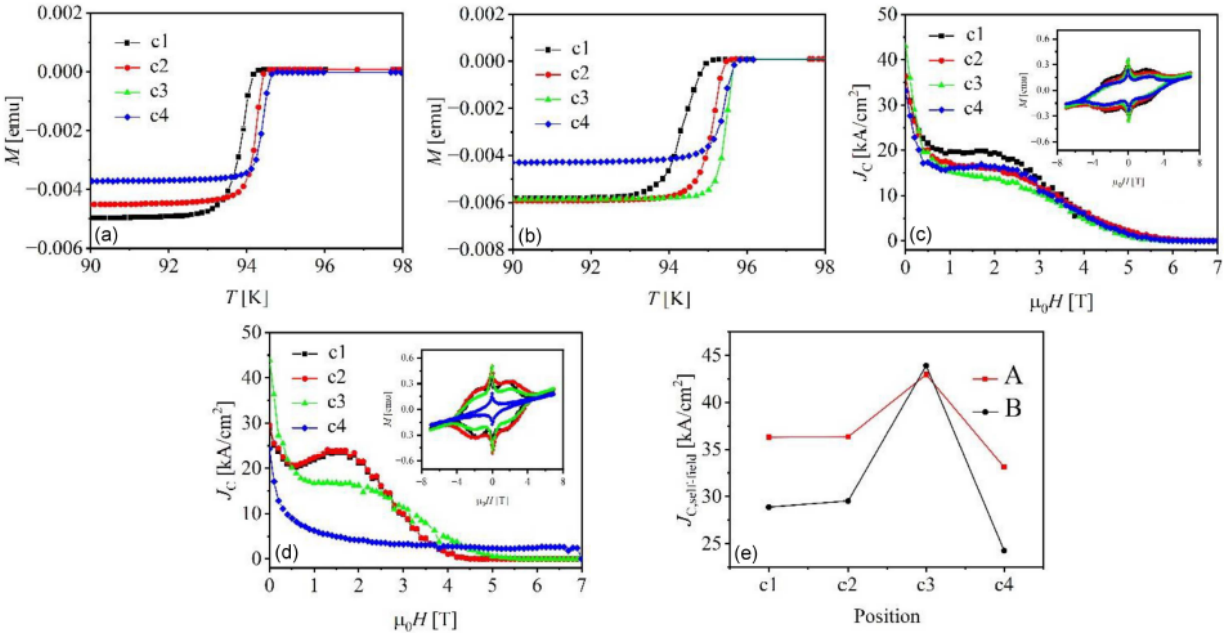

Fig. 4. The temperature dependence of magnetization of specimens in GdBCO superconductor bulks with (a) and without (b) the buffer layer along the c-direction in a ZFC mode under 10 Oe applied fields with $H \parallel c$-axis. The magnetic field $\mu_0 H$ dependence of critical current density J_C of specimens in GdBCO superconductor bulks with (c) and without (d) the buffer layer along the c-direction at 77 K. The insets show magnetic hysteresis loops of specimens in GdBCO superconductor bulks with (c) and without (d) the buffer layer along the c-direction at 77 K. (e) Position dependence of self-field J_C of specimens in GdBCO superconductor bulks with and without the buffer layer along the c-direction.

of the c1 specimen below the seed decreases significantly compared to the other specimens and exhibits a maximum transition width of 2.1 K. The transition width of the c1 specimen after the introduction of the buffer layer reduces to about 1 K. This is due to the direct contact between the seed NdBCO and the GdBCO bulk in bulk B, which contaminated the area near the seed [23, 33]. Due to the lattice mismatch effect, orientation errors and large stresses are easily generated at the interface of the two materials, which leads to the chemical fluctuations of RE/Ba substitution and the formation of cracks, etc., in bulk B. Then the transition width of T_C is increased. The introduction of the buffer layer can also effectively absorb the defects brought about by this lattice mismatch and inhibit their propagation to the interior of the body. Therefore, the specimens in bulk A exhibit T_C values around 94 K and sharp transition widths. However, NdBCO seed contamination mainly affects the area near the seed, and the insertion of the buffer layer absorbs this contamination. The reaction between the MgO substrates of the NdBCO film seed and the buffer layer during the TSMG process leads to the diffusion of the Mg element into the GdBCO bulk [23]. The onset T_C of the specimens in bulk A is around 94 K and lower than that in bulk B, which indicates a uniform distribution of T_C at different locations, as shown in the trapped field in Fig. 3.

Figure 4c and d corresponds to the magnetic field $\mu_0 H$ dependence of critical current density J_C for specimens in the c-direction below the seed at 77 K in bulk A with a buffer layer and bulk B without a buffer layer. The insets show magnetic hysteresis loops of specimens in GdBCO superconductor bulks with (c) and without (d) the buffer layer along the c-direction at 77 K, which are used for calculating J_C in Fig. 4c and d and are common in GdBCO bulks [5]. The self-field J_C values of these specimens are plotted in Fig. 4e in order to clearly illustrate the performance of these specimens in the self-field. Figure 4c shows that the J_C distributions of the specimens in bulk A are almost the same under the applied magnetic field, with a uniform distribution of J_C. The maximum self-field J_C of 4.3×10^4 A/cm^2 is observed for the c3 specimen, while the best J_C performance is seen for the c1 specimen below the seed under the medium field. In contrast to bulk B, specimens c1 and c2 in bulk A did not show a significant second peak effect, which indicates a decrease in Gd/Ba substitution at the corresponding positions and is consistent with the result of T_C [22]. Figure 4d demonstrates that the J_C distribution at various positions in bulk B is noticeably different under the applied magnetic field. The largest self-field J_C of 4.4×10^4 A/cm^2 was measured in specimen c3. In contrast, at mid-field, the c1 and c2 specimens near the seed have the best J_C

performance and show an obvious second peak phenomenon. Based on their wider transition widths, this suggests a certain quantity of Gd/Ba substitutions in the vicinity of the seeds [22], as shown in Fig. 4b. The J_C values of all specimens in bulk A are higher than those of the specimen with corresponding positions in bulk B at a magnetic field of about 4 T and have a high irreversibility field. The J_C performance of the c4 specimen at the bottom of bulk B is obviously decreased, and the J_C value at mid-field is one-fifth of that of the c1 specimen. It indicates that the size of the Gd211 particle phase becomes larger here or the proportion decreases. The buffer-assisted seeding architecture of bulk A enlarges the c-GS volume [29, 30], which is consistent with previous results. From Fig. 4e, it is obvious that the self-field J_C values in the different locations of the c-direction of bulk A with the addition of a buffer layer are higher than those in bulk B. The self-field J_C values have the same variation along the c-direction in bulk A and bulk B, increasing from the c1 position to the c3 position and then decreasing at the c4 position. It can be seen that the introduction of the buffer layer does not change the variation of J_C along the c-direction. The results of the J_C curves show that the buffer layer can lead to a certain improvement in the J_C performance under all fields. Moreover, the uniformity of the J_C distribution in the c-direction is also improved, which is consistent with the good symmetry of the trapped field shown in Fig. 3.

An ideal microstructure is essential for obtaining superior superconductivity in superconductor bulks. Scanning electron microscope photographs at 5000x magnification of specimens c1, c2, c3, and c4 in bulk A with a buffer layer and bulk B without a buffer layer are presented in Fig. 5, where the distribution of the Gd211 particles can be observed. The gray-white particles are Gd211 particles. With the addition of the buffer layer, the distribution of Gd211 particles at different locations in the GdBCO bulk was significantly more uniform. The concentration of Gd211 particles at position c4 in bulk B without a buffer layer decreases dramatically because c4 is located at the bottom of the bulk, which may be related to the end of the growth process, as shown in Fig. 1 and Fig. 4d. In contrast, the concentration of Gd211 particles increased significantly after the addition of the buffer layer (in Fig. 5g), and the corresponding superconducting properties (in Fig. 4c) were also improved. In order to clearly observe the distribution of Gd211 particles, we used ImageJ software to count the size and the fraction of the area occupied by Gd211 particles. Figure 6a shows that the average size of Gd211 along the c-direction in bulk A with the addition of the buffer remarkably decreases, and maintains a similar trend compared with that of bulk B without the addition of the buffer, which first increases slightly and then decreases with increasing distance from the seed, except the slight increase in c4 specimen of

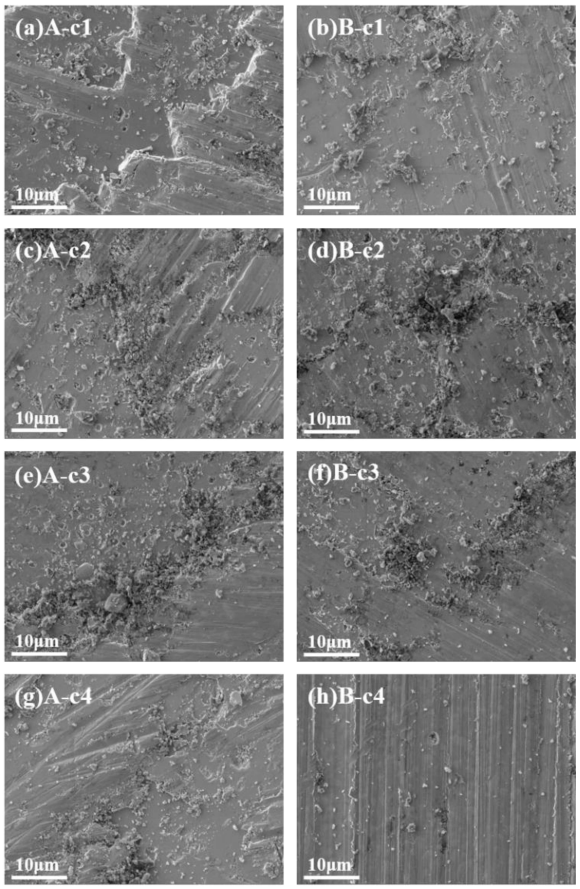

Fig. 5. Scanning electron microscope photographs of specimens in GdBCO superconductor bulks with (bulk A) and without (bulk B) the buffer layer along the c-direction at 5000x magnification.

bulk A. Figure 6b shows that the area fraction occupied by Gd211 particles varies differently along the c-direction in two bulks, i.e., while the area fraction occupied by Gd211 particles in bulk B increases and then decreases along the c-direction, the area fraction occupied by Gd211 particles in bulk A gradually decreases as the distance increases.

The variation trend of Gd211 particles can be extrapolated from the pushing/trapping theory of RE211 solid particles in the liquid phase [34–36]. According to this theory, when RE123 grows and solidifies at a certain rate R, there exists a critical radius r^* for RE211 solid particles, namely

$$R \propto \frac{\Delta\sigma_0}{\eta\, r^*}. \tag{2}$$

In (2), $\Delta\sigma_0$ is the net interface energy of the system, and η is the viscosity coefficient of the liquid phase. When the radius r of RE211 particles in the liquid phase is larger than r^*, the particles are trapped by the RE123 growth front and retained within the RE123 growth zone. If the radius of RE211 particle is smaller than r^*, it will be pushed out by the growth front and will not remain within the growth zone.

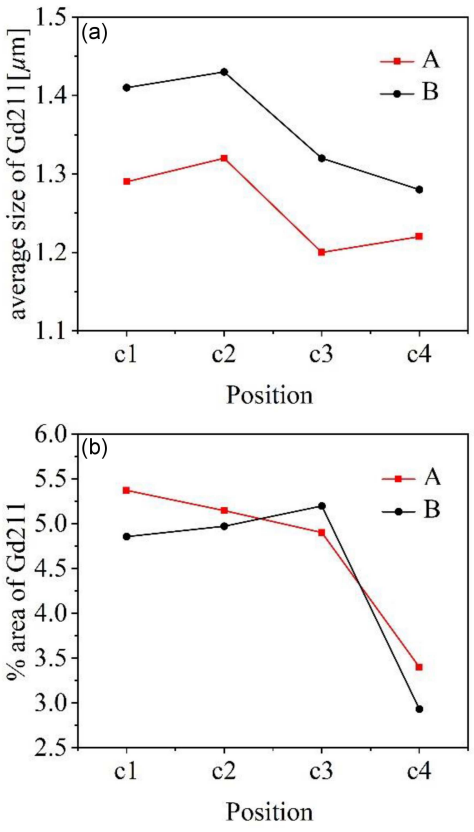

Fig. 6. Distribution of the average size (a) and area occupied by Gd211 particles (b) along the *c*-direction in GdBCO superconductor bulks with (bulk A) and without (bulk B) a buffer layer.

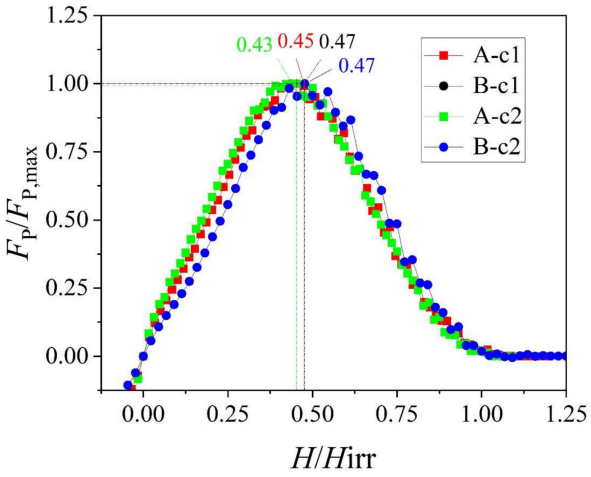

Fig. 7. Normalised functional relationship between pinning force density, $F_p/F_{p,\max}$, and reduction field, H/H_{irr}, of c1 and c2 specimens located below the seeds of GdBCO superconductor bulks with (bulk A) and without (bulk B) a buffer layer at a constant temperature of 77 K.

According to the Ostwald coarsening theory, RE211 particles residing in the liquid phase undergo the Oswald coarsening process. During this process, the smaller-sized RE211 particles dissolve and disappear into the liquid phase, while the dissolved RE^{3+} ions migrate to the larger-sized RE211 particles, allowing further growth and coarsening of the larger particles [37, 38]. The Ostwald coarsening behavior of RE211 particles can be expressed by the formula

$$r_t^3 - r_0^3 = \frac{AD\sigma VC}{RT}\, t, \tag{3}$$

where A is a constant, D is the diffusion coefficient of the liquid phase, σ is the free energy of the RE211/liquid phase interface, V is the volume of 1 mole of RE211 solid particles, C is the concentration of dissolved ions in the liquid phase, R is the gas constant, T is the absolute temperature, t is the residence time of the RE211 particles in the liquid phase, and r_t and r_0 are the average particle radius of the RE211 particles at the moment of t and at the moment of $t = 0$, respectively.

According to the pushing/trapping theory, the growth rate of bulk A with a buffer-assisted structure increases because it can function as a large seed, resulting in a decrease in the net interface energy $\Delta\sigma_0$ of the system, and thereby a decrease in r^*. So the size of trapped Gd211 particles of bulk A decreases and the number increases, indicating that the buffer layer has some effect of refining the Gd211 particles, as shown in Fig. 6a. Smaller Gd211 particles serving as pinning centers [21, 24] improved J_C, so the specimens of bulk A had the best J_C performance, as shown in Fig. 4. At the same time, the area fraction occupied by Gd211 particles of bulk A is larger than that of bulk B, as shown in Fig. 6b, which is related to the improved self-field J_C in bulk A [39]. This is consistent with the results in Fig. 4e.

With the increase in the growth time, the radius of Gd211 particles increases, thus Fig. 6a shows that the size of Gd211 particles at the c2 position increases. It is worth noting that the Gd211 particle size starts to decrease sharply at the c3 position, which is due to two main reasons. Firstly, the c3 specimen is farther away from the seed and has a higher growth rate. According to the pushing/trapping theory, the size of Gd211 particles trapped in the Gd123 growth zone by the growth front decreases. Secondly, the addition of a Y123 liquid phase source reduces the viscosity coefficient of the liquid phase. Therefore, it enlarges the growth rate, and the dissolution rate of Gd211 particles becomes faster, leading to a decrease in the size of Gd211 particles, an increase in their number, and a decrease in the area fraction occupied by Gd211 particles rate. Then, the best J_C performance is in the c3 specimens, as shown in Fig. 4. In addition, the area fraction occupied by Gd211 particles on the c4 specimen at the bottom of both bulks was significantly decreased, which may be related to the exposure to the liquid phase source. The concentration of

Gd211 particles decreases because of the increased concentration of the liquid-rich phase in the microstructure [40]. This is the reason for the sudden decrease in the J_C properties (in Fig. 4e) of the c4 specimen. Although there is not much difference in the size of Gd211 particles between the c4 specimen and the c3 specimen, the superconducting performance of the c4 specimen decreases because of the significant decrease in the area fraction of Gd211 particles, as shown in Fig. 6b.

In order to analyze the effect of the buffer layer structure on the flux-pinning mechanism of the GdBCO bulk superconductors, the normalized pinning force density $F_p/F_{p,\max}$ as a function of reduced field H/H_{irr} at positions c1 and c2 below the seeds in bulks A and B is given in Fig. 7. According to Dew–Hughes [41–46], the peak positions h_0 in the plots represent different superconductor pinning mechanisms, with normal core pinning (δl pinning) denoted when $h_0 \leq 0.3$ and $\Delta\kappa$ core pinning (δT_C pinning) when $h_0 \geq 0.5$. The type δl pinning is caused by non-superconducting particles, but this pinning strength is independent of the nature of the particles. In contrast, the type δT_C pinning is caused by fluctuations in the chemical composition of the superconducting matrix, such as the oxygen-deficient region produced by the insufficient oxygen penetration or the solid solution phase caused by the RE/Ba substitution. The peak positions h_0 of c1 and c2 specimens below the seed of bulk B without a buffer layer are both 0.47, which indicates that dominant δT_C results from the RE/Ba substitution with the obvious second peak effect, as shown in Fig. 4d. After the addition of the buffer layer, the peak positions h_0 of c1 and c2 specimens decreases, which indicates that the δT_C pinning was slightly weakened, accompanied by the disappearing of the second peak effect, as shown in Fig. 4c. Obviously, the normalized pinning force is enhanced at H/H_{irr} less than 0.2 in bulk A with a buffer layer, which is the other evidence of increased δl pinning. The buffer layer has the effect of a large seed, induces the Gd211 particles to be refined and reduces the RE/Ba substitution, supporting our previous discussion.

Figure 8a and b corresponds to the temperature dependence of the magnetization for the first layer of specimens (c1, b1, a1, s1, and t1) along the a/b-direction in, respectively, bulk A and bulk B in a ZFC mode under 10 Oe applied fields with $H \parallel c$-axis. Figure 8c and d corresponds to the temperature dependence of the magnetization for the third layer of specimens (c3, b3, a3, s3, and t3) along the a/b-direction in, respectively, bulk A and bulk B. The results show that the onset transition temperature T_C values of the specimens in the a/b-direction are distributed between 94–96 K, indicating that the prepared GdBCO bulks have excellent superconductivity. In the first layer specimens of bulk A (Fig. 8a), the onset T_C values become larger with increasing distance from the seed, and the largest

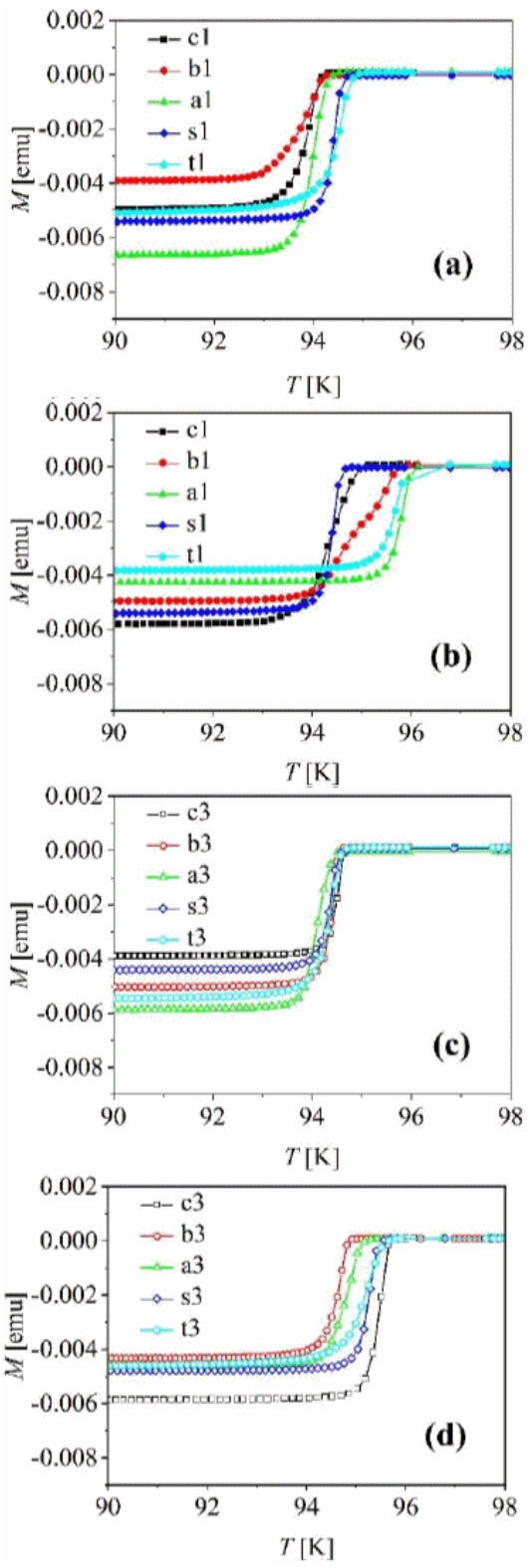

Fig. 8. The temperature dependence of magnetization of specimens in GdBCO superconductor bulks with (bulk A) and without (bulk B) the buffer layer along the a/b-direction in a ZFC mode under 10 Oe applied fields with $H \parallel c$-axis: (a) the first layer specimens in bulk A; (b) the first layer specimens in bulk B; (c) the third layer specimens in bulk A; (d) the third layer specimens in bulk B.

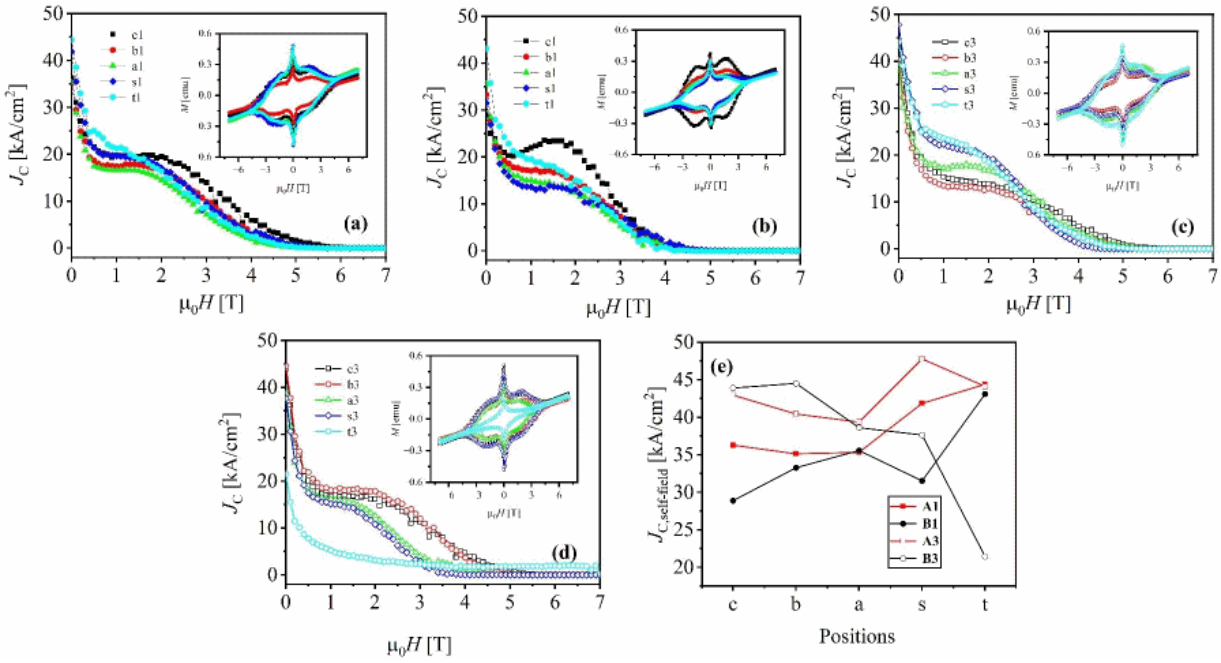

Fig. 9. The magnetic field $\mu_0 H$ dependence of critical current density J_C of specimens in GdBCO superconductor bulks with (bulk A) and without (bulk B) a buffer layer along the a/b-direction at 77 K: (a) the first layer specimens in bulk A; (b) the first layer specimens in bulk B; (c) the third layer specimens in bulk A; (d) the third layer specimens in bulk B. The insets show magnetic hysteresis loops of specimens in GdBCO superconductor bulks with (bulk A) and without (bulk B) the buffer layer along the a/b-direction at 77 K: (a) the first layer specimens in bulk A; (b) the first layer specimens in bulk B; (c) the third layer specimens in bulk A; (d) the third layer specimens in bulk B. (e) Position dependence of self-field J_C of specimens in GdBCO superconductor bulks with and without the buffer layer along the a/b-direction.

onset T_C of 94.9 K is obtained at the bulk edge position t1. Compared to bulk B, the distribution of onset T_C values at different locations in bulk A is more concentrated, and the superconducting transition width is more narrow. The distribution of onset T_C values in the first layer of the specimens in bulk B (Fig. 8b) is relatively dispersed, with the smallest onset T_C at the edge position s1. The transition width of specimen b1 near the seed is the most obvious compared to other specimens, with a transition width value of about 1.8 K. We speculate that the larger transition width observed in specimen b1, which is located near the NdBCO seed in bulk B, may be attributed to an increased RE/Ba substitution [22]. This suggests that the NdBCO seed could contaminate bulk B in the absence of a buffer layer, and the buffer layer plays the role of absorbing the seed contamination, so the transition width of b1 decreases after adding the buffer layer in bulk A. Figure 8c shows that the onset T_C value of the third layer specimen in bulk A is almost the same at 94.6 K and maintains a drastic transition width, which indicates that the distribution of T_C is almost independent of the position. Meanwhile, the T_C distribution of the third layer of specimens in bulk A is significantly more uniform, and all the specimens exhibit a sharp transition width. Overall, the T_C distribution in bulk A is more concentrated, and the transition width varies more drastically. The onset transition temperature of bulk B is relatively high, but the T_C value at different locations is quite different. MgO substrates of NdBCO film seed react with the buffer layer, which results in the penetration of a tiny Mg element to GdBCO bulk during the TSMG process and is responsible for the decline of the onset T_C in bulk A [23]. The addition of a buffer layer resulted in a concentrated distribution of the critical transition temperature T_C at different locations and a decrease in the transition width.

Figure 9 shows the magnetic field $\mu_0 H$ dependence of critical current density J_C for the first layer of specimens (c1, b1, a1, s1, and t1) and the third layer of specimens (c3, b3, a3, s3, and t3) in bulk A and bulk B at 77 K. At the same time, magnetic hysteresis loops for the first layer of specimens (c1, b1, a1, s1 and t1) and the third layer of specimens (c3, b3, a3, s3, and t3) in bulk A and bulk B at 77 K are shown in the inset of Fig. 9a, b, c, and d, which are used for calculating J_C in Fig. 9a, b, c, and d and are common in GdBCO bulks [5]. In order to more visually analyze the distribution of J_C properties in the a/b-direction, we plotted the self-field J_C values of different specimens in Fig. 9e. Figure 9a shows that the J_C distribution of the first layer specimens in bulk A is relatively consistent,

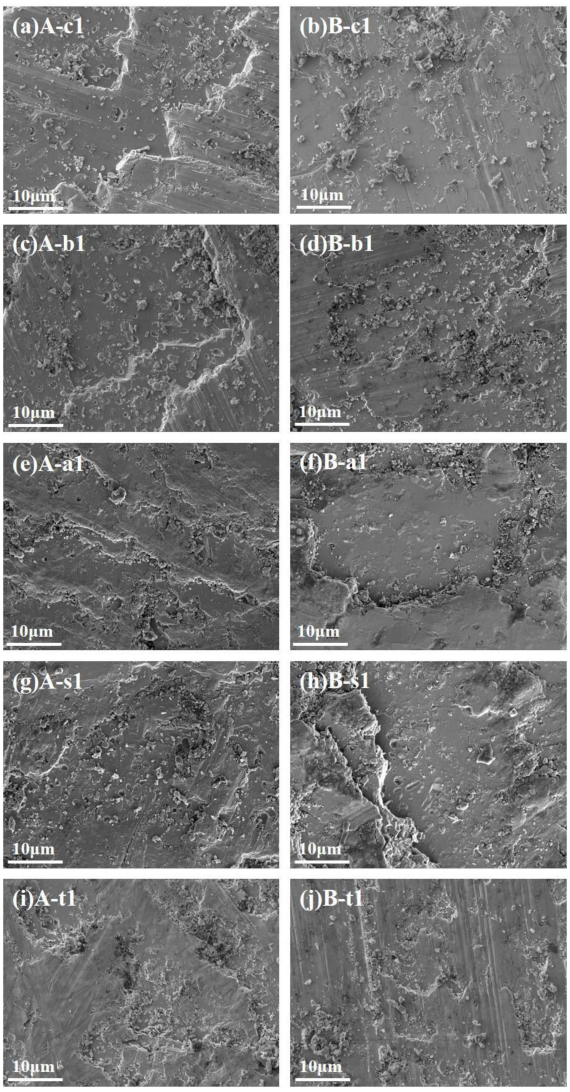

Fig. 10. Scanning electron microscope photographs of the first layer specimens in GdBCO superconductor bulks with (bulk A) and without (bulk B) a buffer layer along the a/b-direction at 5000x magnification.

and there is no obvious second peak effect under the medium field. The self-field J_C value of the specimen t1 at the edge of the bulk is the largest, which is 4.4×10^4 A/cm^2. Compared with that of bulk B, the J_C performance under the middle and high fields obtains some improvements, with a higher irreversibility field. While the J_C distribution of the first layer specimen in bulk B is relatively dispersed, with the largest self-field J_C value at the t1 position, the c1 specimen under the mid-field exhibits an obvious second peak, resulting from the RE/Ba substitution, as shown in Fig. 9b. For the third layer specimens in bulk A in Fig. 9c, the self-field J_C value of s3 near the edge is the highest, and the J_C property near the seed under the mid-field decreases more or less, accompanied by the slight decrease in the spatial uniformity of the J_C distribution. However, as shown in Fig. 9d, from the J_C distribution of the third layer specimens in bulk B, it is obvious that the J_C performance of t3 at the edge position decreased significantly with the lowest self-field J_C value of 2.4×10^4 A/cm^2, and the corresponding T_C transition width increased, which may be related to the end of the growth process or the presence of excess Gd211 phase inclusions. In contrast, the t3 specimen of bulk A showed almost the best J_C performance in all fields. A buffer-assisted seeding architecture reduces the depth of the grain boundary formed by the top surface and the a/c growth sector boundaries [29–31], thus causing a sharp increase in J_C of the t3 specimen in bulk A, which confirms our inference. From Fig. 9e, it is clear that the trend in the self-field J_C values of the first layer specimens in both bulks is similar along the a/b-direction, with an overall increase from the seed to the edge. This means that the J_C values at the edge position of the samples are higher than those of the specimens near the seed, which is a common phenomenon in REBCO superconductor bulks [47]. During the growth of REBCO superconductors, small Gd211 particles in the a/b-direction are similarly pushed to the growth front due to the pushing/trapping theory and coarsening of Gd211 particles, resulting in a general decrease in the size of Gd211 at the edge position. The small Gd211 particles as the pinning center can greatly improve the J_C performance. The self-field J_C values of the third layer specimens in bulk B keep dropping from the seed to the edge. Thus, it suggests that the distribution of microstructures may be different in two layers positions of bulk B, and the distribution of superconducting properties is less homogeneous. Compared with the two bulks, the J_C performance of the specimens in the a/b-direction after the introduction of the buffer layer obtains a certain increase in all fields, and the difference in the J_C distribution between different locations in bulk A is small, and the spatial uniformity of the superconducting properties obtains an increase. However, with the increase in growth depth, there are definite declines in the uniformity.

Figure 10 shows 5000x magnification scanning electron micrographs of the first layer specimens along the a/b-direction in bulk A with a buffer layer and bulk B without a buffer layer. Similarly, we measured the size and area occupied by the Gd211 particles using ImageJ software, and the results are shown in Fig. 11. As shown in Fig. 11a, the size of Gd211 particles in bulk A increases and then decreases along the a/b-direction, reaching a minimum at specimen t1 at the edge of the bulk. However, there is no regularity in the variation of particle size of Gd211 along the a/b-direction in bulk B. The size of Gd211 particles decreases at position b1 near the seed, increases significantly at position s1 near the edge, and then decreases dramatically at position t1 at the edge. This indicates that the size of Gd211 particles at different locations varies considerably,

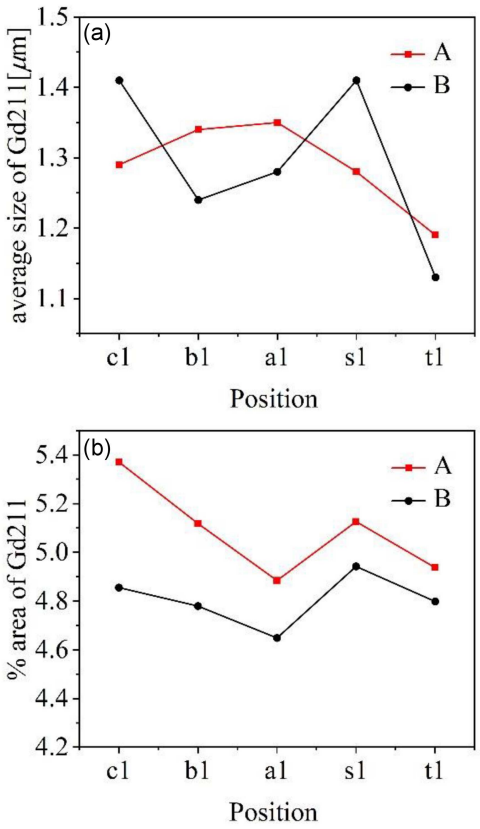

Fig. 11. Distribution of the average size (a) and area occupied by Gd211 particles (b) along the a/b-direction for the first layer of specimens in GdBCO superconductor bulks with (bulk A) and without (bulk B) a buffer layer.

so the local J_C distribution in bulk B is less uniform [39], consistent with the results in Fig. 9b. We suggest that this inhomogeneity may be related to the early stages of growth of the GdBCO superconductor bulks. At the initial stage of melt growth, the growth rate of the Gd123 phase is not stable due to temperature anisotropy, resulting in large variations in the size of the trapped Gd211 particles. The inclusion of a buffer layer may be beneficial in stabilizing the growth rate on the top surface of the bulk so that the size change of Gd211 particles in bulk A is flat, which is related to a relatively uniform distribution of J_C, as shown in Fig. 9a. With the increase in growth time, the size of Gd211 particles increases [37, 38]. Compared to the c1 specimen below the seed, the t1 specimen at the edge of the bulk has a decreased Gd211 particle size, which usually results from the pushing/trapping theory. In turn, this resulted in higher J_C for specimens near the edge than for specimens below the seed. Figure 11b shows that the area fraction occupied by Gd211particles of bulk A and bulk B have the same variation along the a/b-direction, both decreasing and then increasing. This indicates that the number of Gd211 particles decreases at the a1 position and increases at the edge of the bulk. It can be seen that there is an increase in the number of Gd211 particles after the introduction of the buffer layer, which in turn favors the improvement of the J_C performance in the self-field of bulk A [39], as shown in Fig. 9e. The growth rate in the a/b-direction also has some variation in bulk A due to the addition of the buffer layer. Based on the trapping/pushing theory, with the increase in the growth rate, the rate of dissolution of Gd211 particles in the liquid phase increases, resulting in the smaller-sized Gd211 particles in a certain number being trapped in the growth zone.

4. Conclusions

In this study, we successfully prepared two single-domain $GdBa_2Cu_3O_{7-\delta}$ (GdBCO or Gd123) superconductor bulks with (bulk A) and without (bulk B) a buffer layer using the modified top-seeded melt-texture growth (TSMG) method. The buffer layer, consisting of Gd123 and Gd_2BaCuO_5 (Gd211) powders, was pressed into a cylindrical pellet with a diameter of 6 mm and a thickness of 3 mm, which was then inserted between the seed and the precursor. We analyzed the effect of the buffer layer on superconducting properties by investigating trapped flux density, critical temperature (T_C), critical current density (J_C), and microstructure in both bulks. The quadrilateral circle of bulk A is more symmetrical than the triangular circle of bulk B in a two-dimensional (2D) view of the trapped field. The specimens in bulk A have T_C values around 94 K and sharp transition widths. The introduction of the buffer layer can also effectively absorb the defects and inhibit the RE/Ba substitute. Our results showed that the addition of the buffer layer improved the uniformity of J_C distribution along the c-direction, for example, it increased the self-field J_C value from 2.4×10^4 A/cm^2 in c4 below the seed of bulk B to 3.3×10^4 A/cm^2 in c4 below the seed of bulk A. SEM analysis revealed that the size of Gd211 particles along the c-direction decreased, and their area increased after adding the buffer layer. This is because the buffer layer has a large seeding effect, which decreases the net interfacial energy during the growth of the bulk. According to the pushing/trapping theory, the critical radius r^* will decrease under certain growth rate conditions. Then, the Gd211 particle size in bulk A decreases, and the concentration increases. These small and abundant Gd211 particles are beneficial for J_C performance. Furthermore, due to the influence of the buffer layer, the J_C properties of specimens in the a/b-direction were enhanced in all fields and more evenly distributed at different locations. In contrast, the first layer specimen in bulk B exhibited significant variations in Gd211 particle size, with coarsening or refinement at some locations. However, the buffer layer played a role in refining

and uniformizing the distribution of Gd211 particles, which indicates that the buffer layer also positively affects the superconducting properties along the a/b-direction. Therefore, we believe that utilizing a buffer layer improves superconducting properties and microstructural uniformity in GdBCO superconductor bulks by improving the distribution of Gd211 particles. This finding is crucial for preparing high-performance superconductor bulks.

Acknowledgments

This work was supported by the National Natural Science Foundation of China (Grant No. 11004129), the Scientific Research Starting Foundation for the Returned Overseas Chinese Scholars, the Ministry of Education of China (SRF for ROCS, SEM), the Innovation Program of Shanghai Municipal Education Commission, China (Grant No. 11YZ197), the Opening Project of Shanghai Key Laboratory of High-Temperature Superconductors (Grand No. 19DZ2270500).

References

[1] P. Mukherjee, V.V. Rao, *Physica C* **563**, 67 (2019).

[2] P. Peczkowski, P. Szterner, Z. Jaegermann, M. Kowalik, R. Zalecki, W.M. Woch, *J. Supercond. Nov. Magn.* **31**, 2719 (2018).

[3] M. Strasik, J.R. Hull, J.A. Mittleider, J.F. Gonder, P.E. Johnson, K.E. McCrary, C.R. McIver, *Supercond. Sci. Technol.* **23**, (2010).

[4] J. Wang, S. Wang, Y. Zeng et al., *Physica C* **378–381**, 809 (2002).

[5] Y. Zhang, D. Zhou, T. Ida, M. Miki, M. Izumi, *Supercond. Sci. Technol.* **29**, 044005 (2016).

[6] D. Litzkendorf, T. Habisreuther, J. Bierlich, *Supercond. Sci. Technol.* **18**, S206 (2005).

[7] J. Wang, I. Monot, S. Marinel, G. Desgardin, *Mater. Lett.* **33**, 215 (1997).

[8] N.D. Kumar, T. Rajasekharan, R.C. Gundakaram, V. Seshubai, *IEEE Trans. Appl. Supercond.* **21**, 3612 (2011).

[9] S. Meslin, K. Iida, N.H. Babu, D.A. Cardwell, J.G. Noudem, *Supercond. Sci. Technol.* **19**, 711 (2006).

[10] S.P.K. Naik, P. Peczkowski, H. Ogino, M. Muralidhar, N. Sakai, T. Oka, T. Nishio, M. Murakami, *Mater. Chem. Phys.* **272**, 124954 (2021).

[11] A. Cavallaro, F. Sandiumenge, J. Gàzquez, T. Puig, X. Obradors, J. Arbiol, H.C. Freyhardt, *Adv. Funct. Mater.* **16**, 1363 (2006).

[12] M. Fukutomi, Y. Tanaka, T. Asano, H. Maeda, H. Takahara, *MRS Online Proc. Lib.* **169**, 1197 (1989).

[13] A. Goyal, D.P. Norton, D.K. Christen et al., *Appl. Supercond.* **4**, 403 (1996).

[14] X.D. Wu, S.R. Foltyn, P. Arendt, J. Townsend, C. Adams, I.H. Campbell, P. Tiwari, Y. Coulter, D.E. Peterson, *Appl. Phys. Lett.* **65**, 1961 (1994).

[15] D.K. Namburi, Y. Shi, K.G. Palmer, A.R. Dennis, J.H. Durrell, D.A. Cardwell, *Supercond. Sci. Technol.* **29**, 034007 (2016).

[16] P. Yang, J.-F. Fagnard, P. Vanderbemden, W. Yang, *Supercond. Sci. Technol.* **32**, 115015 (2019).

[17] Y. Zhu, Y. Mu, L. Zeng, M. Wang, X. Yao, *Cryst. Growth Design* **20**, 7533 (2020).

[18] Y. Zhu, K. Zmorayová, J. He, Y. Zhang, P. Diko, D. Zhou, X. Yao, *Ceram. Int.* **48**, 22196 (2022).

[19] C.J. Kim, J.H. Lee, S.D. Park, B.H. Jun, S.C. Han, Y.H. Han, *Supercond. Sci. Technol.* **24**, 015008 (2011).

[20] J.H. Lee, S.D. Park, B.H. Jun, J.S. Lee, S.C. Han, Y.H. Han, C.J. Kim, *Supercond. Sci. Technol.* **24**, 055019 (2011).

[21] Y.H. Shi, A.R. Dennis, D.A. Cardwell, *Supercond. Sci. Technol.* **28**, 035014 (2015).

[22] D. Zhou, K. Xu, S. Hara, B. Li, Z. Deng, K. Tsuzuki, M. Izumi, *Supercond. Sci. Technol.* **25**, 025022 (2012).

[23] T.Y. Li, L. Cheng, S.B. Yan, L.J. Sun, X. Yao, Y. Yoshida, H. Ikuta, *Supercond. Sci. Technol.* **23**, 125002 (2010).

[24] D.K. Namburi, Y. Shi, W. Zhai, A.R. Dennis, J.H. Durrell, D.A. Cardwell, *Crys. Growth Design* **15**, 1472 (2015).

[25] M. Eisterer, S. Haindl, T. Wojcik, H.W. Weber, *Supercond. Sci. Technol.* **16**, 1282 (2003).

[26] M. Eisterer, S. Haindl, M. Zehetmayer et al., *Supercond. Sci. Technol.* **19**, S530 (2006).

[27] J. Baumann, Y. Shi, D. Weerakonda, J.H. Durrell, D.A. Cardwell, *J. Eur. Ceram. Soc.* **43**, 1542 (2023).

[28] D.-X. Chen, R.B. Goldfarb, *J. Appl. Phys.* **66**, 2489 (1989).

[29] M.P. Delamare, B. Bringmann, C. Jooss, H. Walter, A. Leenders, H.C. Freyhardt, *Supercond. Sci. Technol.* **15**, 16 (2002).

[30] K. Ozturk, S.B. Guner, M. Abdioglu, M. Demirci, S. Celik, A. Cansiz, *J. Alloys Compd.* **805**, 1208 (2019).

[31] B. Savaskan, S.B. Guner, A. Yamamoto, K. Ozturk, *J. Alloys Compd.* **829**, 154400 (2020).

[32] P. Diko, K. Zmorayová, N.H. Babu, D.A. Cardwell, *Physica C* **398**, 1 (2003).

[33] Y. Shi, J.H. Durrell, A.R. Dennis, Z. Zhang, W. Zhai, N.H. Babu, D.A. Cardwell, *J. Am. Ceram. Soc.* **96**, 1757 (2013).

[34] H.S. Chauhan, T. Egi, A. Endo, Y. Shiohara, *J. Mater. Res.* **11**, 795 (1996).

[35] Y. Shi, D.K. Namburi, W. Zhao, J.H. Durrell, A.R. Dennis, D.A. Cardwell, *Supercond. Sci. Technol.* **29**, (2016).

[36] W. Zhai, Y. Shi, J.H. Durrell, A.R. Dennis, D.A. Cardwell, *Cryst. Growth Design* **14**, 6367 (2014).

[37] S.P. Athur, V. Selvamanickam, U. Balachandran, K. Salama, *J. Mater. Res.* **11**, 2976 (1996).

[38] K. Chan-Joong, H. Gye-Won, *Supercond. Sci. Technol.* **12**, R27 (1999).

[39] V. Antal, K. Zmorayová, M. Rajňak, L. Vojtkova, T. Hlásek, J. Plecháček, P. Diko, *Supercond. Sci. Technol.* **33**, 044004 (2020).

[40] J.V.J. Congreve, Y. Shi, A.R. Dennis, J.H. Durrell, D.A. Cardwell, *Supercond. Sci. Technol.* **30**, 015017 (2017).

[41] D. Dew-Hughes, *Philos. Mag.* **30**, 293 (1974).

[42] K. Rogacki, B. Dabrowski, O. Chmaissem, *Phys. Rev. B* **73**, 224518 (2006).

[43] M.R. Koblischka, A.J.J. van Dalen, T. Higuchi, S.I. Yoo, M. Murakami, *Phys. Rev. B* **58**, 2863 (1997).

[44] A. Hu, H. Zhou, N. Sakai, M. Murakami, *Appl. Phys. Lett.* **81**, 4796 (2002).

[45] A. Hu, N. Sakai, M. Murakami, *Appl. Phys. Lett.* **78**, 2539 (2001).

[46] C.X. Xu, A.M. Hu, N. Sakai, M. Izumi, I. Hirabayashi, *Supercond. Sci. Technol.* **18**, 229 (2005).

[47] C.D. Dewhurst, L. Wai, D.A. Cardwell, *IEEE Trans. Appl. Supercond.* **7**, 1925 (1997).